

## Direct Observation of Vapor–Liquid–Solid Nanowire Growth

Yiying Wu and Peidong Yang\*

Materials Science Division  
Lawrence Berkeley National Laboratory  
Department of Chemistry  
University of California, Berkeley, California 94720

Received December 20, 2000

Nanotubes and semiconductor nanowires are of fundamental importance to the study of size- and dimensionality-dependent chemical and physical phenomena.<sup>1,2</sup> How to rationally synthesize these 1-dimensional nanostructures has been a major challenge, although several strategies have been pursued recently.<sup>3–16</sup> For example, carbon nanotubes have been prepared via condensation of hot carbon plasmas in the presence of certain metals, although the real growth mechanism has been elusive.<sup>3–5</sup> Recently, semiconductor nanowires with different compositions have been successfully synthesized using either vapor<sup>6–12</sup> or solution-based methodologies.<sup>13–16</sup> One key feature of these syntheses is the promotion of anisotropic crystal growth using metal nanoparticles as catalysts. The growth mechanism has been extrapolated from the vapor–liquid–solid (VLS) mechanism which was proposed in the 1960s–1970s for large whisker growth,<sup>17–19</sup> although an oxide-assisted growth mechanism has also been proposed.<sup>2,20</sup> Direct evidence for the nanowire growth mechanism, however, is still lacking except for the fact that these nanowires generally have alloy droplets on their tips. Hence, a better understanding of the nanowire growth process in the vapor phase is necessary to pin down the growth mechanism and to be able to rationally control their compositions, sizes, crystal structures, and growth directions. Herein we report the first real-time observation of semiconductor nanowire growth in an in situ high-temperature transmission electron microscope (TEM), which unambiguously demonstrates the validity of the VLS growth mechanism at

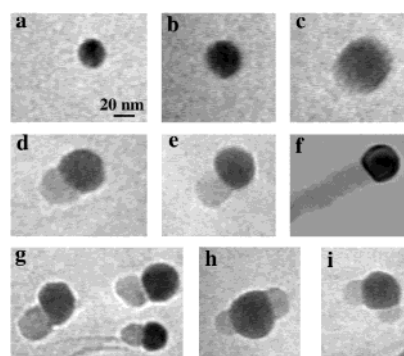


**Figure 1.** In situ TEM images recorded during the process of nanowire growth. (a) Au nanoclusters in solid state at 500 °C; (b) alloying initiates at 800 °C, at this stage Au exists in mostly solid state; (c) liquid Au/Ge alloy; (d) the nucleation of Ge nanocrystal on the alloy surface; (e) Ge nanocrystal elongates with further Ge condensation and eventually a wire forms (f). (g) Several other examples of Ge nanowire nucleation, (h, i) TEM images showing two nucleation events on single alloy droplet.

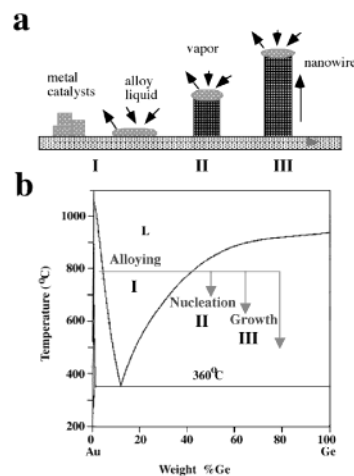


**Figure 2.** (a) Schematic illustration of vapor–liquid–solid nanowire growth mechanism including three stages (I) alloying, (II) nucleation, and (III) axial growth. The three stages are projected onto the conventional Au–Ge binary phase diagram (b) to show the compositional and phase evolution during the nanowire growth process.

nanometer scale.<sup>21</sup> Three well-defined stages have been clearly identified during the process: metal alloying, crystal nucleation, and axial growth. On the basis of this mechanism study, selective growth of Si nanowires with different diameters has been demonstrated using monodispersed gold nanoclusters as catalysts.

In situ observation of wire nucleation/growth at nanometer scale was conducted within a high-temperature transmission electron microscope (JEOL CX200). A small amount of micrometer-sized Ge particles were dispersed on TEM grids together with solution-made monodispersed Au nanoclusters.<sup>22</sup> The gold clusters have average sizes of  $20.2 \pm 3.1$  nm. Although pure Ge has negligible vapor pressure up to 900 °C, we found that a thin layer of carbon coating could promote Ge evaporation within the microscope, presumably due to Ge/C interfacial interaction.<sup>23,24</sup> In fact, prolonged heating of these carbon-coated Ge particles in a vacuum

(1) Hu, J.; Odom, T. W.; Lieber, C. M. *Acc. Chem. Res.* **1999**, *32*, 435–445.

(2) Prokes, S. M.; Wang, K. L. *Mater. Res. Bull.* **1999**, *24*, 13–36.

(3) Colbert, D. T.; Zhang, J.; McClure, S. M.; Nikolaev, P.; Cheng, Z.; Hafner, J. H.; Owens, D. W.; Kotula, P. G.; Carter, C. B.; Weaver, J. H.; Rinzler, A. G.; Smalley, R. E. *Science* **1994**, *266*, 1218–1222.

(4) Cassell, A. M.; Raymakers, J. A.; Kong, J.; Dai, H. J. *J. Phys. Chem. B* **1999**, *103*, 6484–6492.

(5) Bethune, D. S.; Kiang, C. H.; Devries, M. S.; Gorman, G.; Savoy, R.; Vazquez, J.; Beyers, R. *Nature* **1993**, *363*, 605–607.

(6) Morales, A. M.; Lieber, C. M. *Science* **1998**, *279*, 208–210.

(7) Duan, X. F.; Lieber, C. M. *Adv. Mater.* **2000**, *12*, 298–302.

(8) Zhang, Y. F.; Tang, Y. H.; Wang, N.; Yu, D. P.; Lee, C. S.; Bello, I.; Lee, S. T. *Appl. Phys. Lett.* **1998**, *72*, 1835–1837.

(9) Gudiksen, M. S.; Lieber, C. M. *J. Am. Chem. Soc.* **2000**, *122*, 8801–8802.

(10) Wu, Y.; Yang, P. *Chem. Mater.* **2000**, *12*, 605–607.

(11) Tang, C. C.; Fan, S. S.; Dang, H. Y.; Li, P.; Liu, Y. M. *Appl. Phys. Lett.* **2000**, *77*, 1961–1963.

(12) Wang, Z. L.; Dai, Z. R.; Gao, R. P.; Bai, Z. G.; Gole, J. L. *Appl. Phys. Lett.* **2000**, *77*, 3349–3351.

(13) Trentler, T. J.; Hickman, K. M.; Goel, S. C.; Viano, A. M.; Gibbons, P. C.; Buhro, W. E. *Science* **1995**, *270*, 1791–1793.

(14) Trentler, T. J.; Goel, S. C.; Hickman, K. M.; Viano, A. M.; Chiang, M. Y.; Beatty, A. M.; Gibbons, P. C.; Buhro, W. E. *J. Am. Chem. Soc.* **1997**, *119*, 2172–2181.

(15) Heath, J. R.; LeGoues, F. K. *Chem. Phys. Lett.* **1993**, *208*, 263–268.

(16) Holmes, J. D.; Johnson, K. P.; Doty, R. C.; Korgel, B. A. *Science* **2000**, *287*, 1471–1473.

(17) *Whisker Technology*; Levitt, A. P., Ed.; Wiley-Interscience, New York, 1970.

(18) Wagner, R. S.; Ellis, W. C. *Appl. Phys. Lett.* **1964**, *4*, 89–91.

(19) Bootsma, G. A.; Gassen, H. J. *J. Crystal Growth* **1971**, *10*, 223–227.

(20) Wang, N.; Tang, Y. H.; Zhang, Y. F.; Lee, C. S.; Lee, S. T. *Phys. Rev. B* **1998**, *58*, R16024–R16026.

(21) Previously, Wagner has examined the initial growth of whiskers with diameters of 150  $\mu\text{m}$  and identified alloying, whisker nucleation and growth processes (see ref 17).

(22) *Colloidal Gold: Principles, Methods and Applications*; Hayat, M. A., Ed.; Academic Press: New York, 1989.

(23) Lisiecki, I.; Sack-Kongehl, H.; Weiss, K.; Urban, J.; Pileni, M. P. *Langmuir* **2000**, *24*, 8802–8808.

(24) Wu, Y.; Yang, P. *Appl. Phys. Lett.* **2000**, *77*, 43–45.

results in their complete evaporation at 900 °C. Thus, these Ge particles could generate sufficient vapor to condense onto the neighboring Au clusters. During the experiments, the sample stage was heated resistively to 800–900 °C. The real-time evolution of the Au nanoparticle morphology was monitored in bright field mode.

Figure 1a–f shows a sequence of TEM images during the growth of a Ge nanowire in situ. This real-time observation of the nanowire growth directly mirrors the proposed VLS mechanism in Figure 2a. We have examined over 50 individual Au clusters during the in situ catalytic nanowire growth. In general, three stages (I–III) could be clearly identified.

(I): *Alloying process* (Figure 1a–c). Au clusters remain in the solid state up to our maximum experimental temperature 900 °C if there is no Ge vapor condensation. This is confirmed by selected area electron diffraction on the pure Au clusters. With increasing amount of Ge vapor condensation and dissolution, Ge and Au form an alloy and liquefy. The volume of the alloy droplets increases, and the elemental contrast decreases (due to dilution of the heavy metal Au with the lighter element Ge) while the alloy composition crosses sequentially,<sup>25</sup> from left to right, a biphasic region (solid Au and Au/Ge liquid alloy) and a single-phase region (liquid). This alloying process can be depicted as an isothermal line in the Au–Ge phase diagram (Figure 2b).

(II): *Nucleation* (Figure 1d,e). Once the composition of the alloy crosses the second liquidus line, it enters another biphasic region (Au/Ge alloy and Ge crystal). This is where nanowire nucleation starts. Knowing the alloy volume change, we estimate that the nucleation generally occurs at Ge weight percentage of 50–60%. This value differs from the composition calculated from the equilibrium phase diagram which indicates the first precipitation of Ge crystal should occur at 40% Ge (weight) and 800 °C. This difference indicates that the nucleation indeed occurs in a supersaturated alloy liquid.

Interestingly, we have also occasionally observed that two Ge nanocrystals precipitate from single alloy droplets and create two liquid/solid interfaces (Figure 1h,i).<sup>26</sup> The finite volume of the alloy liquid, on the order of  $10^{-17}$  cm<sup>3</sup>, apparently limits the number of possible heterogeneous nucleation events,<sup>27</sup> unlike those microscopic systems where tens or hundreds of whiskers can be observed on single alloy droplet.<sup>17,19</sup>

(III). *Axial growth* (Figure 1d–f). Once the Ge nanocrystal nucleates at the liquid/solid interface, further condensation/dissolution of Ge vapor into the system will increase the amount of Ge crystal precipitation from the alloy. This can be readily accounted for, using the famous lever rule of phase diagram. The incoming Ge species prefer to diffuse to and condense at the existing solid/liquid interface, primarily due to the fact that less energy will be involved with the crystal step growth as compared with secondary nucleation events in a finite volume. Consequently, secondary nucleation events are efficiently suppressed, and no new solid/liquid interface will be created. The existing interface will then be pushed forward (or backward) to form a nanowire (Figures 1f, 2b). After the system cools, the alloy droplets solidify on the nanowire tips. Their compositions were analyzed with energy-dispersive X-ray spectroscopy (EDAX), and it was found that the weight percentage of Ge matches qualitatively well with the estimated alloy composition at which first Ge nanocrystal nucleates.

In addition, by surveying over 50 Au nanocluster-catalyzed Ge nanowire growth processes (Figure 1g), we found that there is a linear correlation between the sizes of Au nanoclusters and the diameters of the Ge nanowires. Generally, the diameters of

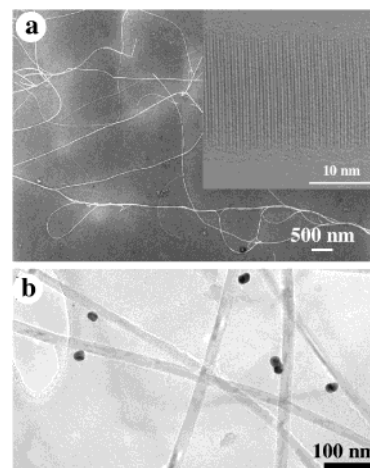


**Figure 3.** (a) FESEM image of Si nanowires grown on Au clusters embedded in a mesoporous silica thin film. Inset shows high-resolution TEM image of individual Si nanowire with the [111] lattice fringe. (b) TEM image of the nanowires and the Au clusters on the same copper grids.

the nanowires are larger than the sizes of the initial clusters by several nanometers due to the Au/Ge alloying process. This size correlation clearly points out a simple approach to selectively grow nanowires of different diameters using monodispersed clusters of different sizes as catalysts.<sup>9,16</sup> We have successfully utilized this strategy to grow uniform Si nanowires in a chemical vapor deposition (CVD) system.<sup>28</sup> For example, uniform nanowires of  $20.6 \pm 3.2$ ,  $24.6 \pm 4.0$ ,  $29.3 \pm 4.5$ , and  $60.7 \pm 6.2$  nm in diameter ( $D_{\text{wires}}$ ) were grown using Au clusters with sizes of  $15.3 \pm 2.4$ ,  $20.1 \pm 3.1$ ,  $25.6 \pm 4.1$ ,  $52.4 \pm 5.3$  nm ( $D_{\text{clusters}}$ ), respectively.<sup>29</sup> Figure 3a shows a field emission scanning electron microscope (FESEM) image of uniform, long, and flexible nanowires grown using 15 nm Au clusters as catalysts. For direct comparison, we deposited the nanowires and nanoclusters on the same TEM grids. Figure 3b indicates an obvious correlation between the starting cluster size and produced nanowire size. These Si nanowires are highly crystalline and generally have [111] growth direction (Figure 3a inset).

The direct observation of nanowire growth unambiguously confirms the validity of vapor–liquid–solid crystal growth mechanism at the nanometer scale and should allow us to rationally control the nanowire growth which is critical for their potential implementation into the nanoscale electronic and optoelectronic devices.

**Acknowledgment.** This work was supported by a Camille and Henry Dreyfus New Faculty Award, Research Corporation, and the University of California, Berkeley. P.Y. is an Alfred P. Sloan Research Fellow. P.Y. thanks the 3M company for an untenured faculty award and thanks Dr. E. Stach and D. C. Nelson for help with the TEM studies. We thank the National Center for Electron Microscopy for the use of their facilities.

JA0059084

(28) The as-made Au clusters<sup>21</sup> were dispersed in a precursor solution for synthesizing mesoporous silica. The precursor solution consists of (molar ratio) 0.01 poly(ethyleneoxide)-*b*-poly(propyleneoxide)-*b*-poly(ethyleneoxide) (EO<sub>20</sub>-PO<sub>70</sub>EO<sub>20</sub>):1 tetraethoxysilane:40 ethanol:0.02 HCl:8 H<sub>2</sub>O (Yang, P. D.; Deng, T.; Zhao, D. Y.; Feng, P. Y.; Pine, D.; Chmelka, B. F.; Whitesides, G. M.; Stucky, G. D. *Science* **1999**, *282*, 2244–2246). A thin film was deposited on a Si wafer using spin coating. The sample was then calcined at 600 °C for 5 h, resulting in a thin mesoporous film embedded with uniform Au clusters. The substrate was then used to grow Si nanowires in a home-built CVD system. Briefly, SiCl<sub>4</sub>/H<sub>2</sub> gas precursors with flow rate of 400 sccm were introduced into a tube reactor at reaction temperature of 965 °C. The growth generally takes 1.5 min. The nanowires were examined by FESEM (JEOL FSM6430) and TEM (Philips CM 200).

(29) A linear correlation can be extrapolated as  $D_{\text{wire}} \text{ (nm)} = 5.0 + D_{\text{clusters}} \text{ (nm)}$ .

(25) Using the densities for solid and liquid Au and Ge, the composition is estimated on the basis of the observed volume change during the alloying process, assuming the droplet is spherical.

(26) For 3 out of 50 examined Au clusters, we observed double nucleation events. No triple-nucleation is observed for these clusters.

(27) Turnbull, D. *J. Appl. Phys.* **1950**, *21*, 1022–1028.